

RESEARCH ARTICLE

**The inverse medium problem in 1D PML-truncated
heterogeneous semi-infinite domains**Jun-Won Kang^a and Loukas F. Kallivokas^{a*}^a*Department of Civil, Architectural and Environmental Engineering,
The University of Texas at Austin, Austin, TX 78712, USA**(June 2009)*

We discuss a total wavefield-based inversion approach for the reconstruction of the material profile of heterogeneous semi-infinite domains, directly in the time domain, based on surficial measurements of the domain's response to prescribed wave illumination. Of particular interest is the ability to recover the in-depth profile of moduli/wave velocities typically associated with geotechnical site characterization applications.

We address four key issues associated with the wavefield-based inversion: a) to limit the semi-infinite extent of the heterogeneous physical domain, a perfectly-matched-layer (PML) is introduced at the truncation interface; b) to account for the introduction of the PML, we use a mixed unsplit-field PML formulation for the coupled PML-regular-domain problem; c) to tackle the inversion, we adopt a partial-differential-equation (PDE)-constrained optimization framework that formally leads to a classic KKT (Karush-Kuhn-Tucker) system comprising the initial-value state, final-value adjoint, and time-independent control problems; and d) to narrow the feasibility space and alleviate the inherent solution multiplicity, we discuss Tikhonov and Total Variation regularization schemes, endowed with a regularization factor continuation algorithm. We also limit the total observation time to optimally account for the domain's heterogeneity during inversion iterations. We report on the theory and results that lead efficiently to the reconstruction of both sharp and smooth profiles in one dimension.

Keywords: inverse medium problem; wave equation; perfectly-matched-layers

AMS Subject Classification: 74J25; 86A22; 35R30; 58J45

1. Introduction

We are concerned with the reconstruction of the spatially-distributed material properties of a heterogeneous elastic medium occupying a semi-infinite domain, by leveraging the medium's response to interrogating waves. The problem is commonly encountered in many science and engineering disciplines, including medical imaging, non-destructive testing, geophysical probing applications, etc. In particular, the problem is of primary importance in geotechnical site characterization investigations for evaluating the mechanical properties (e.g. elastic moduli, attenuation characteristics) of near-surface materials. The latter application is the focus of this article: here, in particular, we describe a systematic methodology and associated numerical results for the one-dimensional case that arises when the stratigraphy is laterally homogeneous, but heterogeneous in depth. Waves are used to probe the stratigraphy by means of an applied excitation (known) at the soil's surface, and the response is recorded directly in the time-domain, also on the surface.

*Corresponding author. Email: loukas@mail.utexas.edu

Mathematically, the problem entails the identification of the spatially dependent coefficients of the (one-dimensional) hyperbolic partial differential equation (PDE) governing the physics of the problem (wave equation). The PDE coefficients may be either continuous or piecewise discontinuous. The problem is often referred to as the inverse medium problem, for it is through knowledge of the source terms (loads) and the medium's response that one seeks to recover the medium's properties. In the last twenty years, such problems have received considerable attention, owing primarily to increased and affordable computational power, as well as to advances in regularization ideas that lend some robustness to the reconstruction algorithms. To date, much of the focus has been on elliptic problems (e.g. see [1]), with only scant attention to hyperbolic problems (e.g. see though [2–5]).

Treatment of the problem at hand can be reduced to addressing two major issues: first, the semi-infinite extent of the physical domain needs to be negotiated in order to arrive at a finite computational domain, especially in light of the heterogeneity and the use of domain numerical methods for resolving the medium's response (here, finite elements). The second issue is the inversion algorithm itself.

To address the first issue, two distinctly different strategies are possible: either to truncate the semi-infinite extent by introducing a transparent condition at the truncation interface, or to truncate by introducing an absorbing condition or absorbing buffer. A transparent condition allows the passage of waves with, ideally, no or minimal reflections from the interface. An absorbing condition will typically force the decay of the wave motion within a buffer zone¹. There are various developments on transparent conditions, broadly classified as either non-local or local, where the non-locality refers to the temporal (convolution) and spatial (boundary integral) response coupling at the truncation interface. Whereas local conditions (e.g. [6–8]) could be cast for arbitrary truncation boundary geometries, exact non-local conditions are only possible for geometries for which the wave equation becomes separable, and of these only a few have been developed (e.g. [9–11]). Both local and non-local transparent conditions are constructed based on the rather constraining assumption of a homogeneous exterior domain (the part of the domain that will be excluded from subsequent computations), which is seldom the case in realistic settings.

By contrast, wave absorbing buffer zones do not suffer from this limitation, and are better able to handle heterogeneity. Among those, the perfectly-matched-layer (PML) is the most widely used absorbing layer scheme, since it has been shown to absorb outgoing waves without generating reflections for all frequencies and angles of incidence [12, 13], even when the medium is heterogeneous. Thus, in this work we favor the PML, and discuss the casting of the inverse problem over a finite computational domain using the PML at the truncation interface boundary. Direct time-domain developments on the PML, which are of interest herein, could be roughly classified as approaches based on split-field (e.g. split[12–14]), and unsplit-field schemes (e.g. [15]). However, none of the prior developments could be easily accommodated within a PDE-constrained optimization framework, which we favor here for dealing with the inverse problem (see discussion below). Specifically, the difficulty with past PML developments arises with adjoint formulations and prevents a systematic treatment. Motivated by this need, we have recently developed ([16]) a new formulation of a mixed unsplit-field PML for one-dimensional elastic, and two-dimensional SH waves, which we adopt here for the resolution of the inverse medium problem.

¹Transparent conditions are sometimes termed absorbing too, and also, silent, non-transmitting, non-reflecting, etc. Here, we adhere to a terminology based on whether there is a zone where the waves are forcibly absorbed (absorbing) or not (transparent).

The second technical issue is the treatment of the inverse problem: here we discuss a partial-differential-equation (PDE)-constrained optimization approach for recovering the spatial variation of the soil's wave velocity profile. We start with the typical misfit between computed and measured responses (in the least-squares sense). The computed response refers to that calculated for a given estimate of the material profile. To satisfy the underlying physics, we construct a Lagrangian functional by augmenting the misfit through the weak imposition of the governing PDEs for the system comprising the regular domain and the PML. This approach is similar to the works by Akcelik et al [2–5], and was originally suggested by Lions [17] in the 1970s. Following classical lines, we seek to reconstruct the profile by requiring that the first-order optimality conditions be satisfied. There result time-dependent state, adjoint, and time-independent control problems, which, upon discretization lead to a classic KKT (Karush-Kuhn-Tucker) system. Here, the state and adjoint problems are initial and final-valued problems, respectively, and both are resolved using a mixed finite element method. We use a reduced-space approach to solve the KKT system, and thus iteratively update the soil's wave velocity profile until convergence. In general, as is usually the case, neither convexity of the Lagrangian functional, nor solution existence and/or uniqueness is guaranteed. Thus, it is necessary to employ specialized regularization schemes to narrow the feasibility space and alleviate difficulties with solution multiplicity. In this work, we report on the performance of Tikhonov (TN) and Total Variation (TV) regularization schemes. We also report numerical results that exhibit successful reconstruction of both smooth and sharp wave velocity profiles based on both noise-free and noisy data.

The combination of a PML in the context of full waveform inversion, with the underlying numerical treatment based on a mixed finite element method, is, to the best of our knowledge, presented here for the first time. Despite the increased computational cost associated with the use of stresses as unknowns (in addition to displacements), a key benefit is the systematic nature of the approach that makes the formulation directly extensible to higher dimensions.

2. Forward wave modeling in a 1D PML-truncated domain

Consider a horizontally-layered, vertically heterogeneous semi-infinite soil medium (Figure 1(a)). We are interested in compressional waves traveling in the layered soil when a uniform stress load $p(t)$ is applied on the entire (two-dimensional) surface. In this setting, the problem can be formally reduced to a one-dimensional problem along the direction of the applied excitation. Similar problems arise if one were to consider only shear waves in the same medium, or compressional waves in a rod. We truncate the semi-infinite domain at $x = L$ as shown in figure 1(b), and introduce a PML wave-absorbing buffer, to arrive at a computationally finite region truncated at $x = L_t$. Figure 1(c) depicts the PML-truncated domain. Typically, the truncation location ($x = L$) is chosen so that it coincides with the region of interest. The outer boundary ($x = L_t$) of the PML is fixed.

In [16], we discussed a mixed displacement-stress formulation that leads to a system of coupled PDEs in the time-domain. Their solution accurately captures the wave motion within the regular domain, while simultaneously enforcing rapid motion attenuation within the PML buffer zone. Here, we repeat for completeness, the main ingredients of the mixed approach to the forward modeling problem. Much of the development hinges on a complex-coordinate stretching concept, whereby the physical coordinate x , is “stretched” to become $\tilde{x} = x - i \frac{c}{\omega} \int_0^x g(s) ds$, where $g(x)$

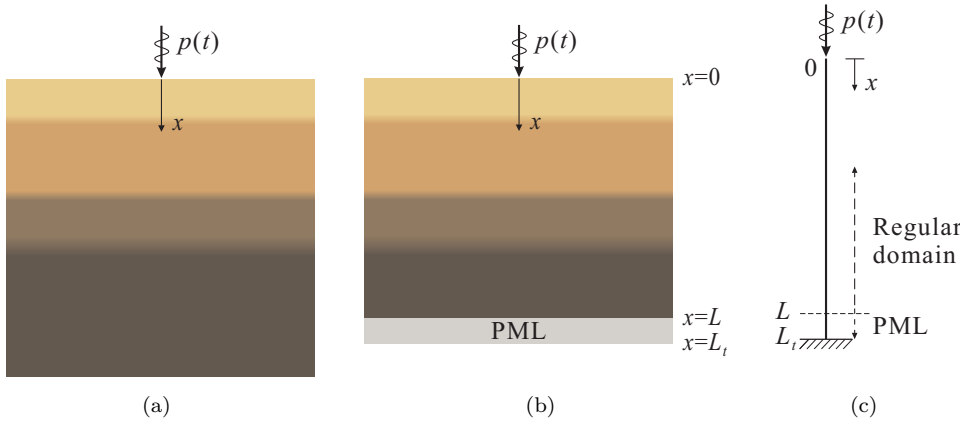


Figure 1. Prototype 1D problem (a) Original domain: horizontally-layered heterogeneous semi-infinite soil medium. (b) PML-truncated finite soil domain. (c) One-dimensional schematic of the PML-truncated domain (PML is placed at $x = L$ and the PML's outer boundary is fixed at $x = L_t$).

is an attenuation function, defined as:

$$g(x) = \begin{cases} 0, & 0 \leq x \leq L \\ \frac{3}{2L_{\text{PML}}} \log\left(\frac{1}{|R|}\right) \left(\frac{x-L}{L_{\text{PML}}}\right)^2, & L \leq x \leq L_t. \end{cases} \quad (1)$$

$L_{\text{PML}} = L_t - L$ is the length of the PML zone, and $c \equiv c(x)$ is the soil's compressional wave velocity, assumed constant within the PML. R is a user-tunable reflection coefficient that controls the amount of reflection from the fixed PML end ($x = L_t$) (see [16] for details). In other words, \tilde{x} is such that $\tilde{x} \equiv x$ within the regular domain, is continuous across the interface between the regular and PML domains (at $x = L$), and is "stretched" within the PML. Then, the *forward problem* becomes:

Find $v \equiv v(x, t)$ and $\sigma \equiv \sigma(x, t)$, such that:

$$\frac{\partial^2 v}{\partial t^2} + cg \frac{\partial v}{\partial t} - \frac{\partial \sigma}{\partial x} = 0, \quad \text{for } x \in (0, L_t), \quad t \in (0, T], \quad (2a)$$

$$\frac{\partial \sigma}{\partial t} + cg\sigma - c^2 \frac{\partial^2 v}{\partial x \partial t} = 0, \quad \text{for } x \in (0, L_t), \quad t \in (0, T], \quad (2b)$$

subject to:

$$v(L_t, t) = 0, \quad (3)$$

$$\sigma(0, t) = p(t), \quad (4)$$

$$v(x, 0) = 0, \quad (5)$$

$$\frac{\partial v}{\partial t}(x, 0) = 0, \quad (6)$$

$$\sigma(x, 0) = 0, \quad (7)$$

where x denotes location and t denotes time. In the above, $v(x, t)$ is a normalized (scalar) displacement with respect to the soil's density ρ , i.e., $v(x, t) = \rho u(x, t)$, in which $u(x, t)$ is the physical displacement. Throughout we assume that the material density is constant (a reasonable assumption in geotechnical site investigations). $\sigma(x, t)$ denotes stress, whose Fourier transform is defined as:

$$\hat{\sigma}(x, \omega) = \rho c^2 \frac{1}{\lambda(x)} \frac{\partial \hat{u}(x, \omega)}{\partial x}, \quad (8)$$

with $\lambda(x)$ denoting the stretch factor:

$$\lambda(x) = 1 - i \frac{g(x)}{\omega}. \quad (9)$$

Equations (2a) and (2b) are the displacement (v) - stress (σ) mixed PML equations governing one-dimensional wave motion in a PML-truncated domain. Within the regular domain, and upon elimination of the stress, the equations reduce to the familiar form of the one-dimensional wave equation. Notice that the mixed PML equations maintain the second-order temporal character of the original wave equation. Condition (3) implies that the PML is fixed at $x = L_t$, whereas condition (4) represents the source excitation $p(t)$ applied at origin. The system is initially at rest by virtue of conditions (5)–(7).

3. The inverse medium problem in a PML-truncated domain

3.1. The misfit problem

The inverse problem targets the reconstruction of the one-dimensional wave velocity profile $c(x)$ within the PML-truncated domain, when given measurements of the medium's response to a known excitation. Accordingly:

Minimize:

$$\mathcal{F} := \frac{1}{2} \int_0^T [v(0, t) - v_m(0, t)]^2 dt + \mathcal{R}(c), \quad (10)$$

subject to (2a), (2b), and (3)–(7).

In (10), \mathcal{F} is the response misfit (in the least-squares sense) augmented by a regularization term $\mathcal{R}(c)$. $v_m(0, t)$ is the measured surface response to the known excitation $p(t)$, and $v(0, t)$ is the computed response corresponding to an assumed model profile $c(x)$. We seek to minimize \mathcal{F} , that is, to force the computed response to match the observation, in an attempt to reconstruct the soil's unknown wave velocity profile $c(x)$. Notice that the minimization problem is subject to the satisfaction of the governing PDEs, initial, and boundary conditions, which describe the underlying physics of the problem. As is well-known, one of the major difficulties of such an inverse problem derives from the fact that there are usually multiple solutions for $c(x)$. Following classical lines, to alleviate the solution multiplicity, we add a regularization term $\mathcal{R}(c)$ to the misfit functional in (10). Two candidate regularization schemes are discussed in the next section.

3.2. Regularization

If data were measured throughout the entire domain, then, the inverse problem could be viewed as a point-to-point matching control problem for which there is a unique solution owing to the linearity of the constraints and the strict convexity of the objective functional [18, 19]. In most inverse problems, however, the observed

data are limited, and the insufficient information will, in general, lead to multiple solutions. The model inverse problem defined in section 3.1 suffers similarly from limited information, since the data are measured only on the top surface of the soil domain. We explore both Tikhonov (TN) [20], and Total Variation (TV) [21] regularization schemes, in an attempt to alleviate ill-posedness.

3.2.1. Tikhonov (TN) regularization:

The Tikhonov-type regularization [20] is one of the most widely-used regularization schemes. It is defined as the L^2 -norm of the gradient of the model parameters. Let $\mathcal{R}^{TN}(c)$ denote the Tikhonov regularization term; then:

$$\mathcal{R}^{TN}(c) := \frac{R_c}{2} \int_0^{L_t} \left(\frac{dc}{dx} \right)^2 dx, \quad (11)$$

where R_c is a scalar, user-defined, regularization factor, which controls the amount of penalty on the gradient of the material parameter $c(x)$. The TN scheme typically enforces smooth spatial variation of the model parameters, since it penalizes the "high-frequency" oscillations of the parameter. Therefore, it is expected that the TN scheme will reconstruct smooth target profiles, but is not expected to perform well in the presence of sharply-varying target profiles, since it tends to smoothen discontinuities.

3.2.2. Total Variation (TV) regularization:

The Total Variation regularization $\mathcal{R}^{TV}(c)$ is defined as:

$$\mathcal{R}^{TV} := R_c \int_0^{L_t} \left[\left(\frac{dc}{dx} \right)^2 + \epsilon \right]^{\frac{1}{2}} dx, \quad (12)$$

where R_c is, again, a regularization factor. \mathcal{R}^{TV} is the bounded variation seminorm of the material parameter $c(x)$, modified by the parameter ϵ . The addition of ϵ makes \mathcal{R}^{TV} differentiable when $dc/dx = 0$. The TV scheme typically preserves jump discontinuities of the material parameter $c(x)$ since, unlike TN, the first variation of \mathcal{R}^{TV} is bounded. At the same time, it penalizes spurious oscillations in smooth regions. Therefore, the TV scheme is expected to perform better when reconstructing sharply-varying profiles than the TN scheme. For both the TN and TV schemes it is important to be able to determine appropriate values for R_c , since the amount of regularization is controlled by the regularization factor (See [22] chapter 7 for a related discussion).

3.3. PDE-constrained optimization

We recast the inverse problem as an unconstrained optimization problem by defining a Lagrangian functional \mathcal{L} , where the objective functional \mathcal{F} is augmented via the weak imposition of the governing PDEs, boundary, and initial conditions:

$$\begin{aligned}
& \mathcal{L}(v, \sigma, \lambda_v, \lambda_\sigma, \lambda_B, \lambda_I, c) \\
&= \frac{1}{2} \int_0^T [v(0, t) - v_m(0, t)]^2 dt + \mathcal{R}_c(c) \\
&+ \int_0^{L_t} \int_0^T \lambda_v \left(\frac{\partial^2 v}{\partial t^2} + cg \frac{\partial v}{\partial t} - \frac{\partial \sigma}{\partial x} \right) dx dt \\
&+ \int_0^{L_t} \int_0^T \lambda_\sigma \left(\frac{\partial \sigma}{\partial t} + cg \sigma - c^2 \frac{\partial^2 v}{\partial x \partial t} \right) dx dt \\
&+ \int_0^T \lambda_B [\sigma(0, t) - f(t)] dt \\
&+ \int_0^{L_t} \lambda_I \frac{\partial v}{\partial t}(x, 0) dx.
\end{aligned} \tag{13}$$

In (13), only Neumann-type boundary and initial conditions have been side-imposed. The remaining boundary condition $v(L_t, t) = 0$, and the two initial conditions $v(x, 0) = 0$, $\sigma(x, 0) = 0$ will be explicitly imposed in the semi-discrete forms. We then seek to satisfy the stationarity of \mathcal{L} , by requiring that the first variations of \mathcal{L} vanish. There result the following first-order optimality conditions:

3.3.1. The first optimality condition:

We enforce the vanishing of the variation of \mathcal{L} with respect to the Lagrange multipliers λ_v , λ_σ , λ_B , λ_I , i.e.,

$$\begin{aligned}
\delta_{\lambda_v} \mathcal{L} &= 0, \\
\delta_{\lambda_\sigma} \mathcal{L} &= 0, \\
\delta_{\lambda_B} \mathcal{L} &= 0, \\
\delta_{\lambda_I} \mathcal{L} &= 0.
\end{aligned} \tag{14}$$

Equations (14) result in the following *mixed state (or forward) problem*, which is the same as the IBVP given by (2a), (2b), and (3)–(7).

State problem

$$\frac{\partial^2 v}{\partial t^2} + cg \frac{\partial v}{\partial t} - \frac{\partial \sigma}{\partial x} = 0, \quad \text{for } x \in (0, L_t), \quad t \in (0, T], \tag{15a}$$

$$\frac{\partial \sigma}{\partial t} + cg \sigma - c^2 \frac{\partial^2 v}{\partial x \partial t} = 0, \quad \text{for } x \in (0, L_t), \quad t \in (0, T], \tag{15b}$$

subject to:

$$v(L_t, t) = 0, \tag{16}$$

$$\sigma(0, t) = p(t), \tag{17}$$

$$v(x, 0) = 0, \tag{18}$$

$$\frac{\partial v}{\partial t}(x, 0) = 0, \tag{19}$$

$$\sigma(x, 0) = 0. \tag{20}$$

3.3.2. The second optimality condition:

Similarly, we require the vanishing of the variation of \mathcal{L} with respect to the state variables v and σ , i.e.,

$$\begin{aligned}\delta_v \mathcal{L} &= 0, \\ \delta_\sigma \mathcal{L} &= 0,\end{aligned}\tag{21}$$

which result in the following *mixed adjoint problem*:

Adjoint problem

$$\frac{\partial^2 \lambda_v}{\partial t^2} - cg \frac{\partial \lambda_v}{\partial t} - \frac{\partial}{\partial x} \left(c^2 \frac{\partial \lambda_\sigma}{\partial t} \right) = 0, \text{ for } x \in (0, L_t), \quad t \in [0, T), \tag{22a}$$

$$\frac{\partial \lambda_\sigma}{\partial t} - cg \lambda_\sigma - \frac{\partial \lambda_v}{\partial x} = 0, \text{ for } x \in (0, L_t), \quad t \in [0, T), \tag{22b}$$

subject to:

$$\lambda_v(L_t, t) = 0, \tag{23}$$

$$c(0)^2 \frac{\partial \lambda_\sigma}{\partial t}(0, t) = v(0, t) - v_m(0, t), \tag{24}$$

$$\lambda_v(x, T) = 0, \tag{25}$$

$$\frac{\partial \lambda_v}{\partial t}(x, T) = 0, \tag{26}$$

$$\lambda_\sigma(x, T) = 0. \tag{27}$$

We remark that the adjoint PDEs (22a) and (22b) have governing operators identical to the state operators in (15a) and (15b), despite the sign reversal of the second terms, and the interchange of the coupling terms (third terms in (22a) and (22b)). Notice also that the adjoint problem is driven by the misfit between the computed and observed responses (24). Therefore, one can solve the adjoint problem for λ_v and λ_σ , once a state solution $v(x, t)$ has been obtained. Lastly, notice from (25)–(27) that the adjoint problem is a final-value problem, as opposed to the initial-value state problem. The adjoint equations are also mixed (λ_v and λ_σ) and PML-endowed.

3.3.3. The third optimality condition:

Lastly, we impose the vanishing of the variation of \mathcal{L} with respect to the material parameter c , i.e.,

$$\delta_c \mathcal{L} = 0, \tag{28}$$

which entails the following time-independent *control problem*:

Control problem

$$-R_c \frac{d^2 c}{dx^2} + \int_0^T \left(g \lambda_v \frac{\partial v}{\partial t} + g \sigma \lambda_\sigma - 2c \lambda_\sigma \frac{\partial^2 v}{\partial x \partial t} \right) dt = 0. \tag{29}$$

In (29), the first term arises when the Tikhonov regularization is used in the augmented Lagrangian functional (13). If, instead, the Total Variation regularization scheme is adopted, the first term in (29) is modified, and the control problem reads:

$$-R_c \epsilon \frac{d^2 c}{dx^2} \left[\left(\frac{dc}{dx} \right)^2 + \epsilon \right]^{-\frac{3}{2}} + \int_0^T \left(g \lambda_v \frac{\partial v}{\partial t} + g \sigma \lambda_\sigma - 2c \lambda_\sigma \frac{\partial^2 v}{\partial x \partial t} \right) dt = 0. \quad (30)$$

Notice that, once the state and adjoint solutions are obtained, the control equation (29) can be used to update the material distribution $c(x)$. We discuss next an iterative procedure, for satisfying the optimality conditions.

4. The inversion process

The stationarity of the augmented Lagrangian functional (13) requires solving the coupled state, adjoint, and control problems defined in the previous section. Whereas all three problems could be solved simultaneously, here we opt for a reduced-space method, whereby the state problem (15a), (15b), (16)–(20) is solved first for a given material property profile. Then, we solve the adjoint problem (22a), (22b), (23)–(27) using the state solutions computed in the previous step, to obtain the adjoint variables λ_v , λ_σ that satisfy the second optimality condition. We use mixed finite elements to solve both state and adjoint problems. As a last step, the material property $c(x)$ is updated in order for the control equation to be satisfied. Notice that the left-hand side of (29) (or (30)) implies the continuous form of the reduced gradient ($\nabla \mathcal{L}$). We use a conjugate gradient method with an inexact line search to iteratively update the material property $c(x)$ using the most recent state and adjoint solutions. The details are discussed in section 4.4.

4.1. Semi-discrete form of the state problem

We employ a mixed finite element method [23–25] to obtain the approximate solutions for the displacement (v) and stress (σ) in the state problem described by the IBVP (15a), (15b), and (16)–(20), where both v and σ are treated as independent variables that need to be approximated separately. We remark that there are two possible variational forms derivable from the mixed equations (15a) and (15b): in the first variational form only the last term in (15a) is integrated by parts. In a second possible variational form it is only the last term in (15b) that is integrated by parts. The resulting two forms differ decidedly in the smoothness requirements they impose on the test and trial functions, with the former requiring less regularity on the stress than the latter. For this reason alone, in this work we opt for the first variational form: accordingly we seek $v \simeq v_h \in H^h \subset H^1(\Omega)$ and $\sigma \simeq \sigma_h \in Q^h \subset L^2(\Omega)$ such that (15a) and (15b) be satisfied. Next, we multiply (15a) and (15b) by appropriate test functions $w(x)$ and $q(x)$, and then integrate over the entire domain $(0, L_t)$ in order to arrive at the corresponding weak forms:

$$\int_0^{L_t} w \left\{ \frac{\partial^2 v}{\partial t^2} + cg \frac{\partial v}{\partial t} \right\} dx + \int_0^{L_t} \frac{dw}{dx} \sigma dx = -w(0)p(t), \quad (31a)$$

$$- \int_0^{L_t} c^2 q \frac{\partial^2 v}{\partial x \partial t} dx + \int_0^{L_t} q \frac{\partial \sigma}{\partial t} dx + \int_0^{L_t} cgq \sigma dx = 0. \quad (31b)$$

In (31a) and (31b), v and σ are approximated as

$$v(x, t) \simeq \phi(x)^T \mathbf{v}(t), \quad \sigma(x, t) \simeq \psi(x)^T \boldsymbol{\sigma}(t), \quad (32)$$

where ϕ and ψ are vectors of approximants associated with nodal displacements $\mathbf{v}(= \rho \mathbf{u})$ and nodal stresses $\boldsymbol{\sigma}$, respectively. The two test functions $w(x)$ and $q(x)$ are similarly approximated by the same approximants ϕ and ψ , respectively, i.e.,

$$w(x) \simeq \mathbf{w}^T \phi(x), \quad q(x) \simeq \mathbf{q}^T \psi(x). \quad (33)$$

To ensure solution stability, the choice of the approximants ϕ and ψ cannot be arbitrary [23, 24]: here we opted for piecewise linear basis functions ϕ and piecewise constant basis functions ψ , which *numerically* have been seen to satisfy the LBB condition [24]. Introducing the approximants in (31a) and (31b) results in the following semi-discrete form¹

$$\begin{aligned} & \begin{bmatrix} \int_0^{L_t} \phi \phi^T dx & \mathbf{0} \\ \mathbf{0} & \mathbf{0} \end{bmatrix} \begin{bmatrix} \ddot{\mathbf{v}} \\ \ddot{\boldsymbol{\sigma}} \end{bmatrix} + \begin{bmatrix} \int_0^{L_t} cg \phi \phi^T dx & \mathbf{0} \\ \int_0^{L_t} -c^2 \psi \frac{\partial \phi^T}{\partial x} dx & \int_0^{L_t} \psi \psi^T dx \end{bmatrix} \begin{bmatrix} \dot{\mathbf{v}} \\ \dot{\boldsymbol{\sigma}} \end{bmatrix} \\ & + \begin{bmatrix} \mathbf{0} & \int_0^{L_t} \frac{\partial \phi}{\partial x} \psi^T dx \\ \mathbf{0} & \int_0^{L_t} cg \psi \psi^T dx \end{bmatrix} \begin{bmatrix} \mathbf{v} \\ \boldsymbol{\sigma} \end{bmatrix} = -p(t) \begin{bmatrix} \phi(0) \\ \mathbf{0} \end{bmatrix}, \end{aligned} \quad (34)$$

Equation (34) can be recast as:

$$\mathbf{M}_{\text{st}} \ddot{\mathbf{u}}_{\text{st}} + \mathbf{C}_{\text{st}} \dot{\mathbf{u}}_{\text{st}} + \mathbf{K}_{\text{st}} \mathbf{u}_{\text{st}} = \mathbf{R}_{\text{st}}, \quad (35)$$

where

$$\mathbf{M}_{\text{st}} \equiv \begin{bmatrix} \mathbf{M}_{\text{st}}^{11} & \mathbf{M}_{\text{st}}^{12} \\ \mathbf{M}_{\text{st}}^{21} & \mathbf{M}_{\text{st}}^{22} \end{bmatrix} = \begin{bmatrix} \int_0^{L_t} \phi \phi^T dx & \mathbf{0} \\ \mathbf{0} & \mathbf{0} \end{bmatrix}, \quad (36)$$

$$\mathbf{C}_{\text{st}} \equiv \begin{bmatrix} \mathbf{C}_{\text{st}}^{11} & \mathbf{C}_{\text{st}}^{12} \\ \mathbf{C}_{\text{st}}^{21} & \mathbf{C}_{\text{st}}^{22} \end{bmatrix} = \begin{bmatrix} \int_0^{L_t} cg \phi \phi^T dx & \mathbf{0} \\ \int_0^{L_t} -c^2 \psi \frac{\partial \phi^T}{\partial x} dx & \int_0^{L_t} \psi \psi^T dx \end{bmatrix}, \quad (37)$$

$$\mathbf{K}_{\text{st}} \equiv \begin{bmatrix} \mathbf{K}_{\text{st}}^{11} & \mathbf{K}_{\text{st}}^{12} \\ \mathbf{K}_{\text{st}}^{21} & \mathbf{K}_{\text{st}}^{22} \end{bmatrix} = \begin{bmatrix} \mathbf{0} & \int_0^{L_t} \frac{\partial \phi}{\partial x} \psi^T dx \\ \mathbf{0} & \int_0^{L_t} cg \psi \psi^T dx \end{bmatrix}, \quad (38)$$

¹We use an overdot to denote differentiation with respect to time when the subtended quantity is a vector (e.g. \mathbf{v}).

$$\mathbf{R}_{\text{st}} = -p(t) \begin{bmatrix} \phi(0) \\ \mathbf{0} \end{bmatrix}, \tag{39}$$

$$\mathbf{u}_{\text{st}} = \begin{bmatrix} \mathbf{v} \\ \boldsymbol{\sigma} \end{bmatrix}. \tag{40}$$

In (35)–(39), \mathbf{M}_{st} , \mathbf{C}_{st} , and \mathbf{K}_{st} represent the mass-like, damping-like, and stiffness-like matrices of the semi-discrete form of the state problem. \mathbf{R}_{st} denotes a load vector. \mathbf{u}_{st} is a vector of nodal unknowns comprising nodal displacement \mathbf{v} and stress $\boldsymbol{\sigma}$. The subscript ‘st’ stands for the *state problem*.

4.2. Semi-discrete form of the adjoint problem

We use again mixed finite elements to resolve the adjoint problem, whereby both λ_v and λ_σ are treated as independent unknowns, and are approximated separately. We use for λ_v and λ_σ the same pair of approximants (linear-constant) as the one we used for v and σ , owing to the similarity of the operators implicated in the state and adjoint problems. In a variational form, only the last term in (22a) is integrated by parts in order to impose less regularity requirement on λ_σ . Accordingly, we seek $\lambda_v \simeq (\lambda_v)_h \in H^h \subset H^1(\Omega)$ and $\lambda_\sigma \simeq (\lambda_\sigma)_h \in Q^h \subset L^2(\Omega)$ such that (22a) and (22b) be satisfied. We multiply (22a) and (22b) by appropriate test functions $w(x)$ and $q(x)$, and then integrate over the entire domain $(0, L_t)$ in order to arrive at the corresponding weak forms:

$$\int_0^{L_t} w \left\{ \frac{\partial^2 \lambda_v}{\partial t^2} - cg \frac{\partial \lambda_v}{\partial t} \right\} dx + \int_0^{L_t} c^2 \frac{\partial \lambda_\sigma}{\partial t} \frac{\partial w}{\partial x} dx = -w(0) [v(0, t) - v_m(0, t)] \tag{41a}$$

$$\int_0^{L_t} q \frac{\partial \lambda_\sigma}{\partial t} dx - \int_0^{L_t} q \frac{\partial \lambda_v}{\partial x} dx - \int_0^{L_t} cgq \lambda_\sigma dx = 0, \tag{41b}$$

where we used $w(L_t) = 0$ and the boundary condition (24). In (41a) and (41b), λ_v and λ_σ are approximated as

$$\lambda_v(x, t) \simeq \boldsymbol{\phi}(x)^T \boldsymbol{\lambda}_v(t), \quad \lambda_\sigma(x, t) \simeq \boldsymbol{\psi}(x)^T \boldsymbol{\lambda}_\sigma(t), \tag{42}$$

where $\boldsymbol{\phi}$ and $\boldsymbol{\psi}$ are vectors of approximants associated with nodal values of λ_v and λ_σ , respectively. The two test functions $w(x)$ and $q(x)$ are similarly approximated by the same approximants $\boldsymbol{\phi}$ and $\boldsymbol{\psi}$, respectively, i.e.,

$$w(x) \simeq \mathbf{w}^T \boldsymbol{\phi}(x), \quad q(x) \simeq \mathbf{q}^T \boldsymbol{\psi}(x). \tag{43}$$

Introducing the approximants in (41a) and (41b) results in the following semi-discrete form for the adjoint problem:

$$\begin{aligned}
& \begin{bmatrix} \int_0^{L_t} \phi \phi^T dx & \mathbf{0} \\ \mathbf{0} & \mathbf{0} \end{bmatrix} \begin{bmatrix} \ddot{\lambda}_v \\ \ddot{\lambda}_\sigma \end{bmatrix} + \begin{bmatrix} -\int_0^{L_t} cg \phi \phi^T dx & \int_0^{L_t} c^2 \frac{\partial \phi}{\partial x} \psi^T dx \\ \mathbf{0} & \int_0^{L_t} \psi \psi^T dx \end{bmatrix} \begin{bmatrix} \dot{\lambda}_v \\ \dot{\lambda}_\sigma \end{bmatrix} \\
& + \begin{bmatrix} \mathbf{0} & \mathbf{0} \\ -\int_0^{L_t} \psi \frac{\partial \phi}{\partial x} dx & -\int_0^{L_t} cg \psi \psi^T dx \end{bmatrix} \begin{bmatrix} \lambda_v \\ \lambda_\sigma \end{bmatrix} = -[v(0, t) - v_m(0, t)] \begin{bmatrix} \phi(0) \\ \mathbf{0} \end{bmatrix} \quad (44)
\end{aligned}$$

Equation (44) can be recast as:

$$\mathbf{M}_{\text{adj}} \ddot{\mathbf{u}}_{\text{adj}} + \mathbf{C}_{\text{adj}} \dot{\mathbf{u}}_{\text{adj}} + \mathbf{K}_{\text{adj}} \mathbf{u}_{\text{adj}} = \mathbf{R}_{\text{adj}}, \quad (45)$$

where

$$\mathbf{M}_{\text{adj}} \equiv \begin{bmatrix} \mathbf{M}_{\text{adj}}^{11} & \mathbf{M}_{\text{adj}}^{12} \\ \mathbf{M}_{\text{adj}}^{21} & \mathbf{M}_{\text{adj}}^{22} \end{bmatrix} = \begin{bmatrix} \int_0^{L_t} \phi \phi^T dx & \mathbf{0} \\ \mathbf{0} & \mathbf{0} \end{bmatrix}, \quad (46)$$

$$\mathbf{C}_{\text{adj}} \equiv \begin{bmatrix} \mathbf{C}_{\text{adj}}^{11} & \mathbf{C}_{\text{adj}}^{12} \\ \mathbf{C}_{\text{adj}}^{21} & \mathbf{C}_{\text{adj}}^{22} \end{bmatrix} = \begin{bmatrix} -\int_0^{L_t} cg \phi \phi^T dx & \int_0^{L_t} c^2 \frac{\partial \phi}{\partial x} \psi^T dx \\ \mathbf{0} & \int_0^{L_t} \psi \psi^T dx \end{bmatrix}, \quad (47)$$

$$\mathbf{K}_{\text{adj}} \equiv \begin{bmatrix} \mathbf{K}_{\text{adj}}^{11} & \mathbf{K}_{\text{adj}}^{12} \\ \mathbf{K}_{\text{adj}}^{21} & \mathbf{K}_{\text{adj}}^{22} \end{bmatrix} = \begin{bmatrix} \mathbf{0} & \mathbf{0} \\ -\int_0^{L_t} \psi \frac{\partial \phi}{\partial x} dx & -\int_0^{L_t} cg \psi \psi^T dx \end{bmatrix}, \quad (48)$$

$$\mathbf{R}_{\text{adj}} = -[v(0, t) - v_m(0, t)] \begin{bmatrix} \phi(0) \\ \mathbf{0} \end{bmatrix}, \quad (49)$$

$$\mathbf{u}_{\text{adj}} = \begin{bmatrix} \lambda_v \\ \lambda_\sigma \end{bmatrix}, \quad (50)$$

where the subscript ‘adj’ stands for the *adjoint problem*. \mathbf{M}_{adj} , \mathbf{C}_{adj} , and \mathbf{K}_{adj} represent the mass-like, damping-like, and stiffness-like matrices of the adjoint semi-discrete equations. \mathbf{R}_{adj} denotes the adjoint load vector. \mathbf{u}_{adj} is a vector of nodal unknowns comprising Lagrange multipliers λ_v and λ_σ . We remark that all adjoint-problem matrices can be constructed from their state-problem counterparts, since:

$$\begin{aligned}
\mathbf{M}_{\text{adj}}^{ij} &= \mathbf{M}_{\text{st}}^{ij}, & (i, j) &= (1, 1), (1, 2), (2, 1), (2, 2), \\
\mathbf{C}_{\text{adj}}^{ij} &= -\left(\mathbf{C}_{\text{st}}^{ji}\right)^{\text{T}}, & (i, j) &= (1, 1), (1, 2), (2, 1), \\
\mathbf{C}_{\text{adj}}^{22} &= \mathbf{C}_{\text{st}}^{22}, \\
\mathbf{K}_{\text{adj}}^{11} &= \mathbf{K}_{\text{st}}^{11}, \\
\mathbf{K}_{\text{adj}}^{ij} &= -\left(\mathbf{K}_{\text{st}}^{ji}\right)^{\text{T}}, & (i, j) &= (1, 2), (2, 1), (2, 2).
\end{aligned} \tag{51}$$

The above relations greatly aid in reducing the computational cost of the entire inversion process, since the assembly of the adjoint matrices at every inversion iteration is readily available. Despite the lack of symmetry of $\mathbf{K}_{\text{st}/\text{adj}}$ and $\mathbf{C}_{\text{st}/\text{adj}}$, the semi-discrete forms can be easily integrated using standard schemes; we discuss the time integration next.

4.3. State and adjoint problem time integration

4.3.1. Integration of the state semi-discrete forms:

Use of Newmark's average acceleration scheme yields the following linear system of equations for the state unknowns \mathbf{u}_{st} at the $(n + 1)$ -th time step:

$$\mathbf{K}_{\text{st}}^{\text{eff}} \mathbf{u}_{\text{st}}^{n+1} = \left[\mathbf{R}_{\text{st}}^{\text{eff}}\right]^{n+1}, \tag{52}$$

where the state effective stiffness matrix $\mathbf{K}_{\text{st}}^{\text{eff}}$ and the effective load vector $\left[\mathbf{R}_{\text{st}}^{\text{eff}}\right]^{n+1}$ are given as:

$$\mathbf{K}_{\text{st}}^{\text{eff}} = \frac{4}{\Delta t^2} \mathbf{M}_{\text{st}} + \frac{2}{\Delta t} \mathbf{C}_{\text{st}} + \mathbf{K}_{\text{st}}, \tag{53}$$

$$\begin{aligned}
\left[\mathbf{R}_{\text{st}}^{\text{eff}}\right]^{n+1} &= \mathbf{R}_{\text{st}}^{n+1} + \mathbf{M}_{\text{st}} \left(\frac{4}{\Delta t^2} \mathbf{u}_{\text{st}}^n + \frac{4}{\Delta t} \dot{\mathbf{u}}_{\text{st}}^n + \ddot{\mathbf{u}}_{\text{st}}^n \right) \\
&\quad + \mathbf{C}_{\text{st}} \left(\frac{2}{\Delta t} \mathbf{u}_{\text{st}}^n + \dot{\mathbf{u}}_{\text{st}}^n \right),
\end{aligned} \tag{54}$$

In the above Δt denotes time step. Once $\mathbf{u}_{\text{st}}^{n+1}$ is obtained from (52), the velocities $\dot{\mathbf{u}}_{\text{st}}^{n+1}$ and accelerations $\ddot{\mathbf{u}}_{\text{st}}^{n+1}$ can be computed as:

$$\dot{\mathbf{u}}_{\text{st}}^{n+1} = \frac{2}{\Delta t} \left(\mathbf{u}_{\text{st}}^{n+1} - \mathbf{u}_{\text{st}}^n \right) - \dot{\mathbf{u}}_{\text{st}}^n, \tag{55}$$

$$\ddot{\mathbf{u}}_{\text{st}}^{n+1} = \frac{4}{\Delta t^2} \left(\mathbf{u}_{\text{st}}^{n+1} - \mathbf{u}_{\text{st}}^n \right) - \frac{4}{\Delta t} \dot{\mathbf{u}}_{\text{st}}^n - \ddot{\mathbf{u}}_{\text{st}}^n. \tag{56}$$

4.3.2. Integration of the adjoint semi-discrete forms:

We use the average acceleration rule for the time integration of semi-discrete adjoint equations as well. Starting from the final conditions (25)–(27), the semi-

discrete form (44) should be resolved for nodal adjoint unknowns \mathbf{u}_{adj} at each time step, by marching in decreasing times along the time line. We set:

$$\mathbf{u}_{\text{adj}}^{n-1} = \mathbf{u}_{\text{adj}}^n - \frac{\Delta t}{2} \left(\dot{\mathbf{u}}_{\text{adj}}^n + \dot{\mathbf{u}}_{\text{adj}}^{n-1} \right), \quad (57)$$

$$\dot{\mathbf{u}}_{\text{adj}}^{n-1} = \dot{\mathbf{u}}_{\text{adj}}^n - \frac{\Delta t}{2} \left(\ddot{\mathbf{u}}_{\text{adj}}^n + \ddot{\mathbf{u}}_{\text{adj}}^{n-1} \right). \quad (58)$$

Equations (57) and (58) can be solved for $\dot{\mathbf{u}}_{\text{adj}}^{n-1}$ and $\ddot{\mathbf{u}}_{\text{adj}}^{n-1}$, respectively, to provide:

$$\dot{\mathbf{u}}_{\text{adj}}^{n-1} = -\frac{2}{\Delta t} \left(\mathbf{u}_{\text{adj}}^{n-1} - \mathbf{u}_{\text{adj}}^n \right) - \dot{\mathbf{u}}_{\text{adj}}^n, \quad (59)$$

$$\ddot{\mathbf{u}}_{\text{adj}}^{n-1} = \frac{4}{\Delta t^2} \left(\mathbf{u}_{\text{adj}}^{n-1} - \mathbf{u}_{\text{adj}}^n \right) + \frac{4}{\Delta t} \dot{\mathbf{u}}_{\text{adj}}^n - \ddot{\mathbf{u}}_{\text{adj}}^n. \quad (60)$$

On the other hand, the equations of motion (45) at the $(n-1)$ -th time step can be written as:

$$\mathbf{M}_{\text{adj}} \ddot{\mathbf{u}}_{\text{adj}}^{n-1} + \mathbf{C}_{\text{adj}} \dot{\mathbf{u}}_{\text{adj}}^{n-1} + \mathbf{K}_{\text{adj}} \mathbf{u}_{\text{adj}}^{n-1} = \mathbf{R}_{\text{adj}}^{n-1}. \quad (61)$$

Substituting (59) and (60) into (61) and rearranging the terms, we arrive at the following system of equations at the $(n-1)$ -th time step:

$$\mathbf{K}_{\text{adj}}^{\text{eff}} \mathbf{u}_{\text{adj}}^{n-1} = \left[\mathbf{R}_{\text{adj}}^{\text{eff}} \right]^{n-1}, \quad (62)$$

where the adjoint effective stiffness matrix $\mathbf{K}_{\text{adj}}^{\text{eff}}$ and the effective load vector $\left[\mathbf{R}_{\text{adj}}^{\text{eff}} \right]^{n-1}$ are:

$$\mathbf{K}_{\text{adj}}^{\text{eff}} = \frac{4}{\Delta t^2} \mathbf{M}_{\text{adj}} - \frac{2}{\Delta t} \mathbf{C}_{\text{adj}} + \mathbf{K}_{\text{adj}}, \quad (63)$$

$$\begin{aligned} \left[\mathbf{R}_{\text{adj}}^{\text{eff}} \right]^{n-1} &= \mathbf{R}_{\text{adj}}^{n-1} + \mathbf{M}_{\text{adj}} \left(\frac{4}{\Delta t^2} \mathbf{u}_{\text{adj}}^n - \frac{4}{\Delta t} \dot{\mathbf{u}}_{\text{adj}}^n + \ddot{\mathbf{u}}_{\text{adj}}^n \right) \\ &\quad + \mathbf{C}_{\text{adj}} \left(-\frac{2}{\Delta t} \mathbf{u}_{\text{adj}}^n + \dot{\mathbf{u}}_{\text{adj}}^n \right). \end{aligned} \quad (64)$$

Notice that $\mathbf{K}_{\text{adj}}^{\text{eff}}$ and $\left[\mathbf{R}_{\text{adj}}^{\text{eff}} \right]^{n-1}$ are identical to $\mathbf{K}_{\text{st}}^{\text{eff}}$ and $\left[\mathbf{R}_{\text{st}}^{\text{eff}} \right]^{n+1}$ in (53) and (54), provided Δt is set to $-\Delta t$. Once $\mathbf{u}_{\text{adj}}^{n-1}$ is obtained from (62), the adjoint velocities $\dot{\mathbf{u}}_{\text{adj}}^{n-1}$ and accelerations $\ddot{\mathbf{u}}_{\text{adj}}^{n-1}$ can be computed using (59) and (60).

4.4. Material parameter updates

By solving the state and adjoint problems as described in section 4.3, the first and second optimality conditions are automatically satisfied. There remains to update the material property in order to satisfy the third optimality condition

(control problem). Clearly, only the true/target profile satisfies exactly the control equations (29) (or, (30), if the Total Variation regularization is used). We note though that the left-hand side of the control equation is the reduced gradient of the augmented Lagrangian functional ($\nabla_c \mathcal{L}$), which is equal to the gradient of the objective functional ($\nabla_c \mathcal{F}$), since the side constraints in (13) have already vanished owing to the satisfaction of the state problem. Thus, the reduced gradient has the following continuous form derivable from (29) ($g \equiv 0$ in the regular domain):

$$\begin{aligned} \nabla_c \mathcal{L} &= -R_c \frac{d^2 c}{dx^2} - 2c \int_0^T \left(\lambda_\sigma \frac{\partial^2 v}{\partial x \partial t} \right) dt \\ &= -R_c \frac{d^2 c}{dx^2} - \frac{2}{c} \int_0^T \left(\lambda_\sigma \frac{\partial \sigma}{\partial t} \right) dt, \end{aligned} \quad (65)$$

in the case of Tikhonov regularization, and is replaced by the left-hand side of (30) if the Total Variation regularization scheme is used. The continuous form of the reduced gradient is discretized by evaluating it at each nodal point. Since we use linear basis functions to interpolate v and λ_v , nodal values for v , \dot{v} , and λ_v are directly available from the state and adjoint discrete solutions. However, the values of σ and λ_σ are available only per element since constant basis functions are used to approximate them. Therefore, we evaluate nodal values of σ and λ_σ by taking the average of the values from the elements surrounding the node. For the left-most and right-most nodes, the nodal stress term is taken to be one half of the value of the element adjacent to the node. The nodal g value can be directly calculated by its definition (1). The second derivative $d^2 c/dx^2$ and the first derivative $\partial \dot{v}/\partial x$ at each nodal point are evaluated by second-order accurate finite difference schemes. Once the discrete reduced gradient is calculated, we seek the nodal values of the material property $c(x)$, such that the objective functional \mathcal{F} be minimized. Details on how to iteratively approach the solution are discussed below based on a conjugate gradient method with inexact line search.

4.4.1. Conjugate gradient method

Let us denote by \mathbf{g}_k the discrete reduced gradient at the k -th inversion iteration:

$$\mathbf{g}_k = (\nabla_c \mathcal{L})_k. \quad (66)$$

We also denote by \mathbf{c}_k the material property vector comprising nodal values of $c(x)$ at the k -th iteration. The number of elements in \mathbf{g}_k and \mathbf{c}_k is the same as the number of nodes. We use a conjugate gradient method (Fletcher-Reeves) to update \mathbf{c}_k ; accordingly:

$$\mathbf{c}_{k+1} = \mathbf{c}_k + \alpha \mathbf{d}_k, \quad (67)$$

where \mathbf{d}_k is the search direction at \mathbf{c}_k , and α is the step length in the direction of \mathbf{d}_k . The search direction \mathbf{d}_k is determined as:

$$\mathbf{d}_k = \begin{cases} -\mathbf{g}_k & (k = 0), \\ -\mathbf{g}_k + \frac{\mathbf{g}_k \cdot \mathbf{g}_k}{\mathbf{g}_{k-1} \cdot \mathbf{g}_{k-1}} \mathbf{d}_{k-1} & (k \geq 1). \end{cases} \quad (68)$$

We evaluate the misfit functional (10) using the updated material property \mathbf{c}_{k+1} ,

Table 1. Algorithm 1: Backtracking line search procedure

Choose $\bar{\alpha} > 0$, $\rho, \mu \in (0, 1)$; set $\alpha \leftarrow \bar{\alpha}$;
repeat
 $\alpha \leftarrow \rho\alpha$;
until $\mathcal{F}(\mathbf{c}_k + \alpha\mathbf{d}_k) \leq \mathcal{F}(\mathbf{c}_k) + \mu\alpha\mathbf{g}_k \cdot \mathbf{d}_k$
 Terminate with $\alpha_k = \alpha$

Table 2. Algorithm 2: Inversion algorithm using a mixed unsplit-field PML scheme; reduced space approach

1: Choose $\bar{\alpha}$, ρ , μ , and R_c ; Set $\alpha = \bar{\alpha}$
 2: Set $k=0$ and convergence tolerance tol
 3: Set initial guess of material property vector \mathbf{c}_k
 4: Set $\mathcal{F}_m = tol + 1$
 5: **while** ($\mathcal{F}_m > tol$) **do**
 6: Solve the state problem (15a), (15b), (16)–(20) and obtain v and σ
 7: Solve the adjoint problem (22a), (22b), (23)–(27) and obtain λ_v and λ_σ
 8: Compute the discrete form of the reduced gradient $\mathbf{g}_k = (\nabla_c \mathcal{L})_k$
 9: Compute the search direction \mathbf{d}_k ((68))
 10: **while** [$\mathcal{F}(\mathbf{c}_k + \alpha\mathbf{d}_k) \geq \mathcal{F}(\mathbf{c}_k) + \mu\alpha\mathbf{g}_k \cdot \mathbf{d}_k$] **do**
 11: $\alpha \leftarrow \rho\alpha$
 12: **end while**
 13: Update material property vector by $\mathbf{c}_{k+1} = \mathbf{c}_k + \alpha\mathbf{d}_k$
 14: $k = k + 1$
 15: **end while**

and compare it against a preset tolerance. If the tolerance threshold is not met, we set $k \leftarrow k + 1$, and proceed to the next iteration. As is known, the search direction \mathbf{d}_k will be progressively contaminated by errors resulting from the inaccuracies involved in the determination of α , and by the round-off error involved in the accumulation of the $\mathbf{g}_k \cdot \mathbf{g}_k / \mathbf{g}_{k-1} \cdot \mathbf{g}_{k-1}$ terms in (68) [26]. Hence, in practice, it is necessary that \mathbf{d}_{m+1} be set equal to $-\mathbf{g}_{m+1}$ after every m step instead of the usual form (we used $m = 10$).

One can also find an optimal step length α as the local minimizer in the direction of \mathbf{d}_k , but it is generally too expensive to compute it. More practical strategies perform an inexact line search to determine a step length that achieves adequate reductions in the objective functional \mathcal{F} .

4.4.2. Inexact line search – sufficient decrease and backtracking

A popular inexact line search condition requires that α force sufficient decrease in the objective functional \mathcal{F} , as measured by the following inequality:

$$\mathcal{F}(\mathbf{c}_k + \alpha\mathbf{d}_k) \leq \mathcal{F}(\mathbf{c}_k) + \mu\alpha\mathbf{g}_k \cdot \mathbf{d}_k, \quad (69)$$

(*Armijo condition* or *sufficient decrease condition*). In practice, μ is chosen to be quite small ([27]; herein, we used $\mu = 10^{-8}$). In order to opt for a step length α satisfying (69), we use the so-called *backtracking* approach as summarized in Table 1. In this procedure, the initial step length $\bar{\alpha}$ is usually fixed. If (69) is violated, an acceptable step length α will be found after a finite number of trials by setting $\alpha \leftarrow \rho\alpha$, such that α becomes small enough to satisfy the Armijo condition ($\rho = 0.5$ is a typical value). We summarize the entire inversion process discussed so far in Table 2.

4.5. Regularization factor continuation

When calculating the reduced gradient $\nabla_c \mathcal{L}$ in (65), the choice of the regularization factor (R_c) is of importance since it controls the amount of imposed penalty on high frequency oscillations of the material properties. Though mindful of various developments (e.g. L-curve [28, 29]), here we opted for a simple and practical approach, which we describe next. The objective functional \mathcal{F} (10) can be formally re-written as:

$$\mathcal{F} = \mathcal{F}_m + \mathcal{R}(c), \quad (70)$$

where

$$\mathcal{F}_m = \frac{1}{2} \int_0^T [v(0, t) - v_m(0, t)]^2 dt, \quad (71)$$

$$\mathcal{R}(c) = R_c \mathcal{F}_r(c). \quad (72)$$

Here, \mathcal{F}_m and \mathcal{F}_r denote the misfit and the regularization functional, respectively, and R_c is the regularization factor. Recall that the reduced gradient of the augmented Lagrangian functional ($\nabla_c \mathcal{L}$) is tantamount to the gradient of the objective functional ($\nabla_c \mathcal{F}$). With this in mind, we can recast equation (65) as:

$$\nabla_c \mathcal{L} = R_c (\nabla_c \mathcal{F}_r) + (\nabla_c \mathcal{F}_m), \quad (73)$$

where

$$\nabla_c \mathcal{F}_r = -\frac{d^2 c}{dx^2}, \quad (74)$$

$$\nabla_c \mathcal{F}_m = -\frac{2}{c} \int_0^T \left(\lambda_\sigma \frac{\partial \sigma}{\partial t} \right) dt. \quad (75)$$

In (75), $\nabla_c \mathcal{F}_r$ is the gradient of the regularization functional, and $\nabla_c \mathcal{F}_m$ is the gradient of the misfit functional. $\nabla_c \mathcal{F}_r$ penalizes high frequency fluctuations in the recovered profile, such that, the higher R_c is, the smoother the reconstructed profile becomes. R_c can have a fixed value throughout the inversion process. However, sharp profiles may not be recoverable if R_c is too large, or the inversion process may suffer from solution multiplicity if R_c is too small. Therefore, there is a need to continuously modify the regularization factor to avoid such difficulties. We suggest the following criterion to determine the regularization factor at each inversion iteration:

$$\text{Impose } R_c |\nabla \mathcal{F}_r| < |\nabla \mathcal{F}_m| \Rightarrow R_c < \frac{|\nabla \mathcal{F}_m|}{|\nabla \mathcal{F}_r|}. \quad (76)$$

In this work, R_c is chosen, at each iteration, to be:

$$R_c = \frac{1}{2} \frac{|\nabla \mathcal{F}_m|}{|\nabla \mathcal{F}_r|}. \quad (77)$$

Equation (77) enables the regularization part (first term) in (73) to compete with

the misfit part (second term) through the entire inversion process without hindering the overall direction of the material property. By the continuation scheme, the regularization factor can take a large value at the beginning of the inversion process to assist in narrowing down the initial feasibility space of the solution. It is also continuously reduced as the inversion process progresses so as to enable the reconstruction of sharply varying profiles.

5. Numerical examples

We discuss next numerical results obtained using the procedure outlined in the preceding sections. We consider first a heterogeneous semi-infinite soil medium as shown in figure 2(a), and assume that the soil's material property varies only with depth as is the case with horizontally-layered media. We model the medium as a one-dimensional PML-truncated domain, with the regular domain occupying $0\text{m} \leq x < 100\text{m}$, and the PML layer placed at $100\text{m} \leq x \leq 110\text{m}$, as shown in figure 2(b). Figure 2(c) is the target wave velocity profile, which has a smooth variation along the entire domain. Notice that the profile is homogeneous within the PML. We apply a stress $p(t)$ on the surface ($x = 0$), realized via a short pulse-type load as depicted in figure 3(a). Figure 3(b) depicts the frequency spectrum of the excitation. Figure 3(c) shows the measured displacement response $v(0, t)$ on the surface, which we obtained by solving the forward problem using a fine mesh density, and a distant placement of the truncation boundary to avoid committing an inverse "crime."

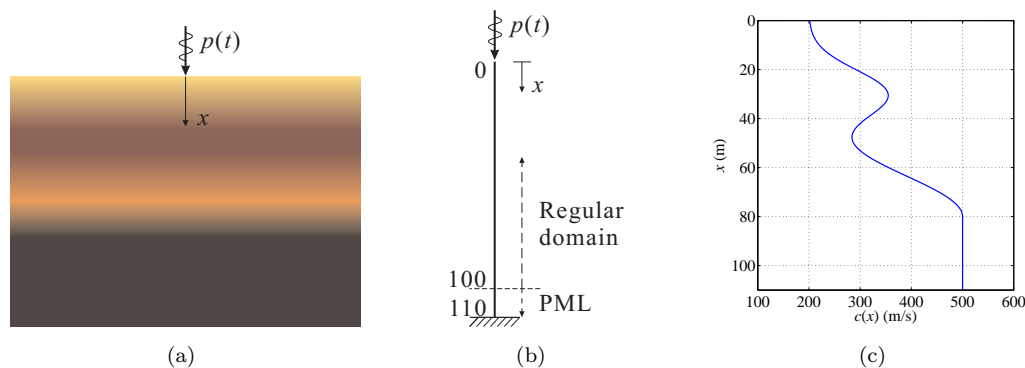


Figure 2. (a) Heterogeneous semi-infinite soil medium; (b) corresponding one-dimensional PML-truncated semi-infinite domain; (c) target, smooth, wave velocity profile $c(x)$

Figure 4 shows the reconstructed wave velocity profiles (red dots) of the layered soil medium using the Tikhonov regularization scheme. The inversion process started with a homogeneous initial guess of 200 (m/s) (green dots) and regularization factors (a) $R_c = 10^{-6}$, and (b) $R_c = 10^{-8}$. The true profile (blue line) is recovered fairly well for both regularization cases with a relatively better outcome in the case of the smaller regularization factor ($R_c = 10^{-8}$). Figure 5 shows similar inversion results when the Total Variation regularization scheme is used. We remark that both the TN and TV schemes capture the smooth target velocity profile very well.

We turn next to sharp profiles. Figure 6 depicts a 5-layer soil with sharp interfaces between the layers. We apply the same stress load $p(t)$ on the surface ($x = 0$) as before, and obtain again the measured displacement response $v(0, t)$ (Figure 7). We use again a homogeneous initial guess of 200 m/s, and recover the 5-layer velocity

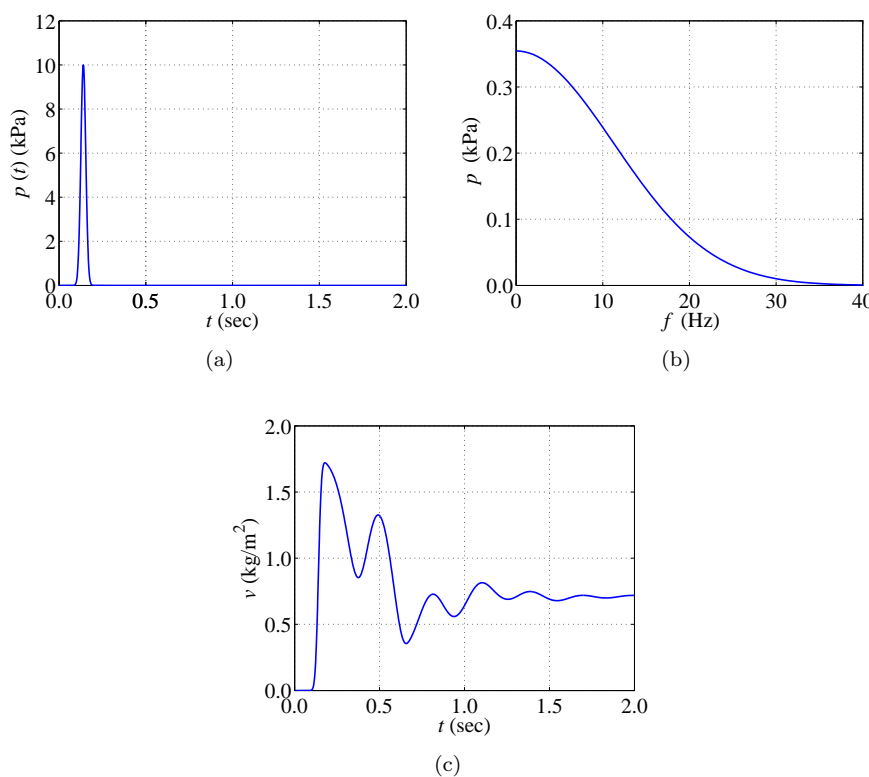


Figure 3. (a) Time history of the applied stress $p(t)$. (b) Frequency spectrum of the applied stress $p(t)$. (c) Measured displacement response $v(0,t)$ ($= \rho u(0,t)$).

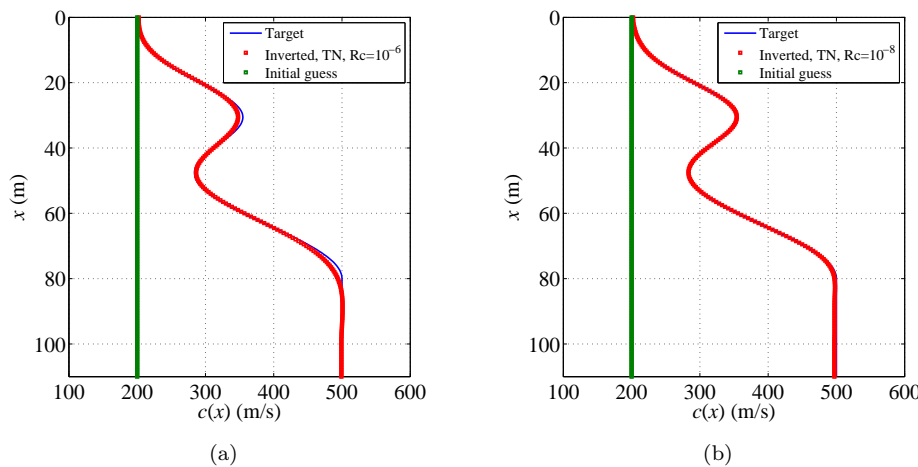


Figure 4. Initial guess, target, and inverted wave velocity profiles using Tikhonov regularization with: (a) $R_c = 10^{-6}$, and (b) $R_c = 10^{-8}$; both results were obtained using 3760 iterations.

profile using TN and TV regularization schemes with two different regularization factors ($R_c = 10^{-6}$ and $R_c = 10^{-8}$), as shown in figure 8. Both schemes recovered the true profile fairly well. Of interest here is the ability to recover the sharp discontinuities in the target profile. Notice that, as shown in figure 8(a), the TV regularization scheme captures the sharply varying profile reasonably well, while the TN regularization scheme smoothens out discontinuities. This is due to the fact that the TN regularization scheme imposes higher penalty on the gradient of the properties than the TV regularization when the regularization factor (R_c) is

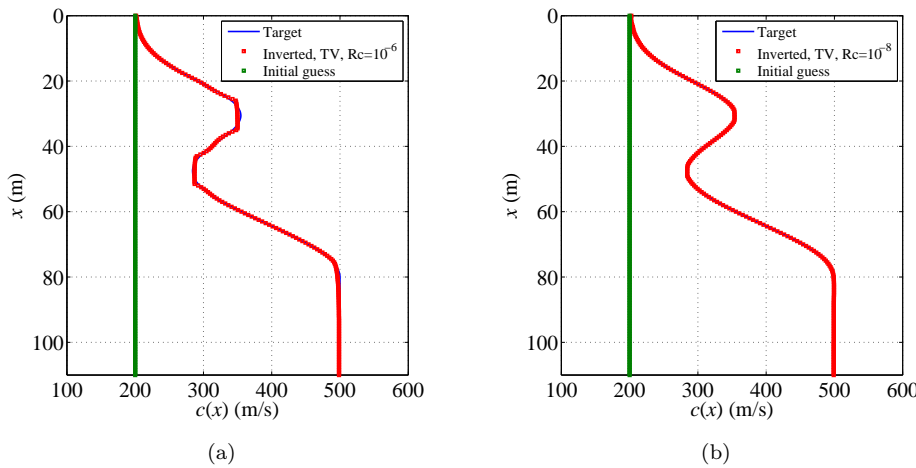


Figure 5. Initial guess, target, and inverted wave velocity profiles using Total Variation regularization with: (a) $R_c = 10^{-6}$, and (b) $R_c = 10^{-8}$; both results were obtained using 5000 iterations.

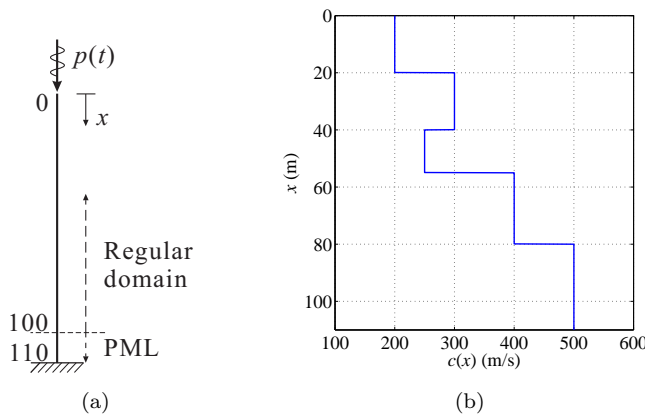


Figure 6. A target wave velocity profile with 5 layers.

the same. If the regularization factor becomes smaller, the penalty effect on the gradient of the properties is diminished so that both schemes show little difference, as it can be seen in figure 8(b) ($R_c = 10^{-8}$). In this case, however, the recovered profile exhibits more oscillation, especially in flat regions, than in the case of a larger regularization factor.

In general, the regularization factor R_c needs to be large at the beginning of the inversion process to assist in narrowing down the initial feasibility space of the solution. However, as it can be seen in figure 8(a), if the regularization factor does not change, the reconstruction of sharply varying profiles will be somewhat hindered. We use the regularization factor continuation scheme described in section 4.5 to overcome this difficulty. Figure 9 compares the fixed regularization scheme against the continuous regularization, by attempting to reconstruct again the target layered profile shown in figure 6. The initial guess is again a homogeneous 200 m/s, and the TN regularization is used. The continuation scheme starts with the same $R_c = 10^{-6}$ as the fixed scheme, but shows better performance in recovering the layered profile.

We consider next the effect of noise in the inversion process. To this end, Figure 10 depicts the measured displacement response $v(0, t)$ with 20% Gaussian noise. The target velocity profile is again the 5-layer profile shown in figure 6(b), and the

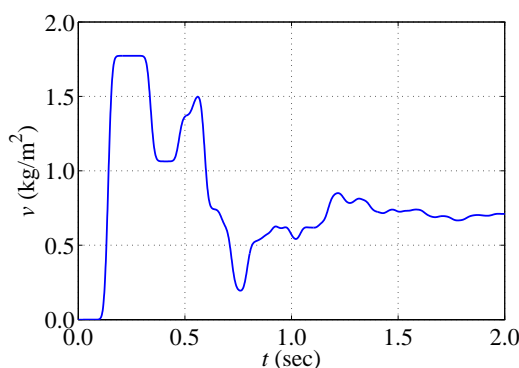


Figure 7. Measured displacement response $v(0, t)$. Data are obtained by applying the stress load $p(t)$ presented in figure 3(a) on the 5-layer profile depicted in figure 6(b).

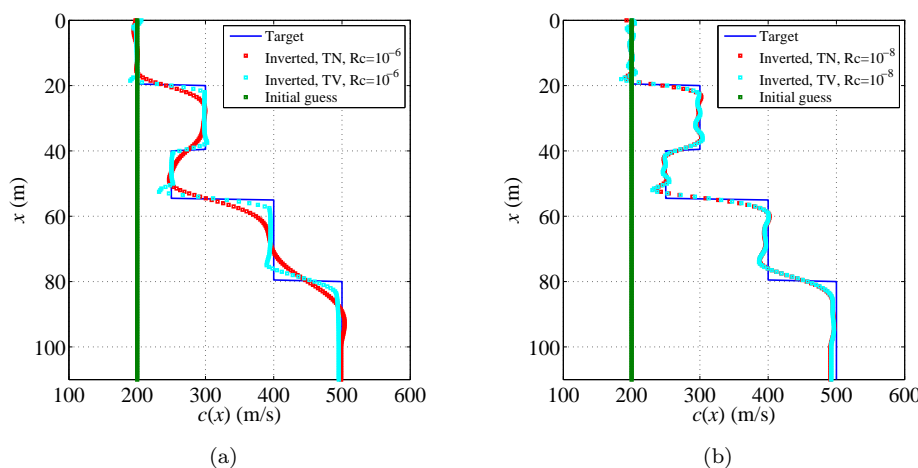


Figure 8. Inverted sharp 5-layer profile using Tikhonov and Total Variation regularization with: (a) $R_c = 10^{-6}$, and (b) $R_c = 10^{-8}$; both results were obtained using 2660 iterations.

applied load is the one depicted in figures 3(a) and 3(b). We explore again the TN and TV regularization schemes with two different fixed regularization factors ($R_c = 10^{-6}$, 10^{-8}). Figure 11 shows the inverted profiles for each regularization factor. It is interesting to note that, for $R_c = 10^{-6}$, the TN scheme captures the layered profile as a smooth interpolant would do, without allowing much fluctuation in the properties even in the presence of as much as 20% noise in the measured data. By contrast, the TV scheme is affected highly by noise. For $R_c = 10^{-8}$, both schemes exhibit material oscillations, since the effect of the regularization has been lessened owing to the smaller R_c .

5.1. PML placement

It is of interest to explore the effect the PML location has on the quality of the reconstructed profiles. Ideally, the PML should be placed at a depth beyond which one could ascertain homogeneity, since in this way the entire heterogeneous region will be contained within the computational domain. However, such *a priori* knowledge is rarely available. If, on the other hand, the PML is placed at a location that leaves portion of the heterogeneous region outside the computational domain, and if the observation period is such that information from the deeper layers are accounted for in the surface response, then the profile reconstruction stands to be

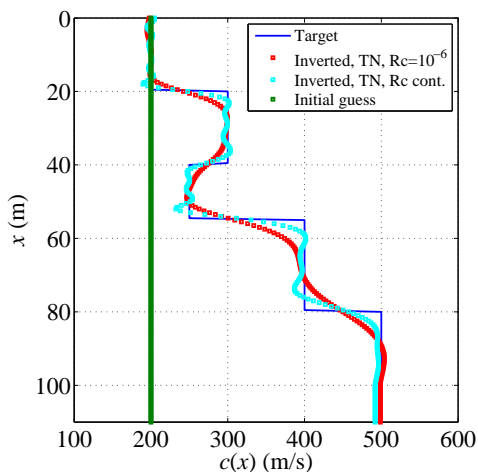


Figure 9. Inverted sharp 5-layer profile using Tikhonov regularization; fixed regularization factor versus regularization factor continuation scheme.

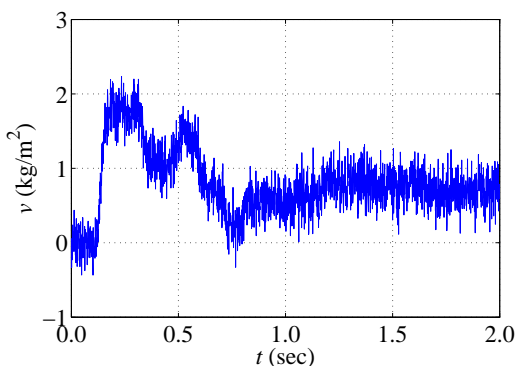


Figure 10. Measured displacement response $v(0, t)$ with 20% Gaussian noise. Data are obtained by applying the stress load $p(t)$ presented in figure 3(a) on the 5-layer profile depicted in figure 6(b).

polluted.

In [30], it was shown that by limiting the observation period, and by iteratively relocating the truncation interface, convergence to a common profile is attainable. Here, we show that limiting the observation period is sufficient for attaining quality profiles, without having to iteratively relocate the PML. This is, by and large, due to the wave-absorbing nature of the PML, as opposed to the truncating (wave-passing) nature of the local truncation conditions we used in [30], which causes reflections in the presence of heterogeneity. Specifically:

Given a measured response $v_m(0, t)$, we seek to limit the observation period based on wave travel times. The optimal observation period is set equal to the travel time it will take for the wave to travel down and up the truncated (regular) domain, augmented by the excitation duration t_d . In this way, we expect that, roughly, information up to only the truncation depth will be taken into account when working with the measured response¹. The detailed process is summarized below:

- (1) First, we truncate the domain and place the PML at an arbitrary depth $x = L$. The target profile is assumed to be homogeneous, i.e., $c(x) = c^{(0)}$,

¹This is not entirely true during the early inversion iterations due to the difference between the working and true profiles.

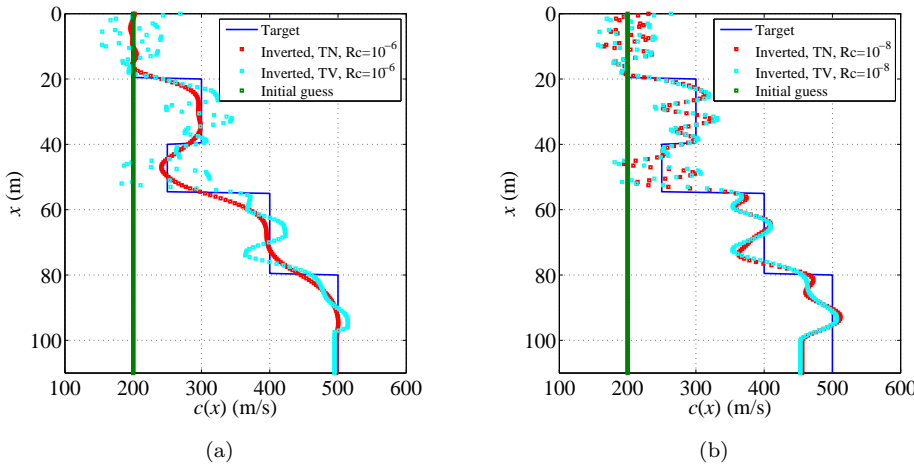


Figure 11. Inverted 5-layer profile using measured data with 20% Gaussian noise. Both TN and TV regularization schemes were used with: (a) $R_c = 10^{-6}$, and (b) $R_c = 10^{-8}$.

and the observation period $T^{(0)}$ is defined as:

$$T = T^{(0)} = t_d + 2 \frac{L}{c^{(0)}}. \quad (78)$$

- (2) Next, we invert for the material profile by using the observation period T , and obtain the, in general, inhomogeneous distribution $c^{(1)}(x)$.
- (3) Next, using the new profile, we update the observation period such that:

$$T^{(k)} = t_d + 2 \int_0^L \frac{1}{c^{(k)}(x)} dx, \quad (79)$$

where k denotes the k -th inversion iteration ($k \geq 1$). The last two steps are repeated until convergence.

We seek to reconstruct the layered profile depicted in figure 6 using the above scheme for various truncation depths, without making any *a priori* assumption on profile homogeneity beyond the truncation depth. We use the same stress load $p(t)$ as before (Fig. 3(a)) and use both noise-free and noisy data (Figs. 7 and 10, respectively). We place the PML at various depths ($l = 30\text{m}, 50\text{m}, 70\text{m}, 100\text{m}$) and set the observation time based on (79). Figure 12 depicts the inverted profiles for each of the truncation cases starting with an initial (homogeneous) guess of 200 m/s and noise-free data. The results of the profile reconstruction are remarkably good regardless of the truncation depth. Clearly, limiting the observation period, per the outlined scheme, allows the *arbitrary* placement of the PML, at the truncation depth of choice/interest. When there is 20% Gaussian noise in the measured response, the reconstructed profiles become polluted, especially near the surface. Nevertheless, as depicted in figure 13, the reconstructed profiles still follow quite closely, albeit roughly, the target profiles.

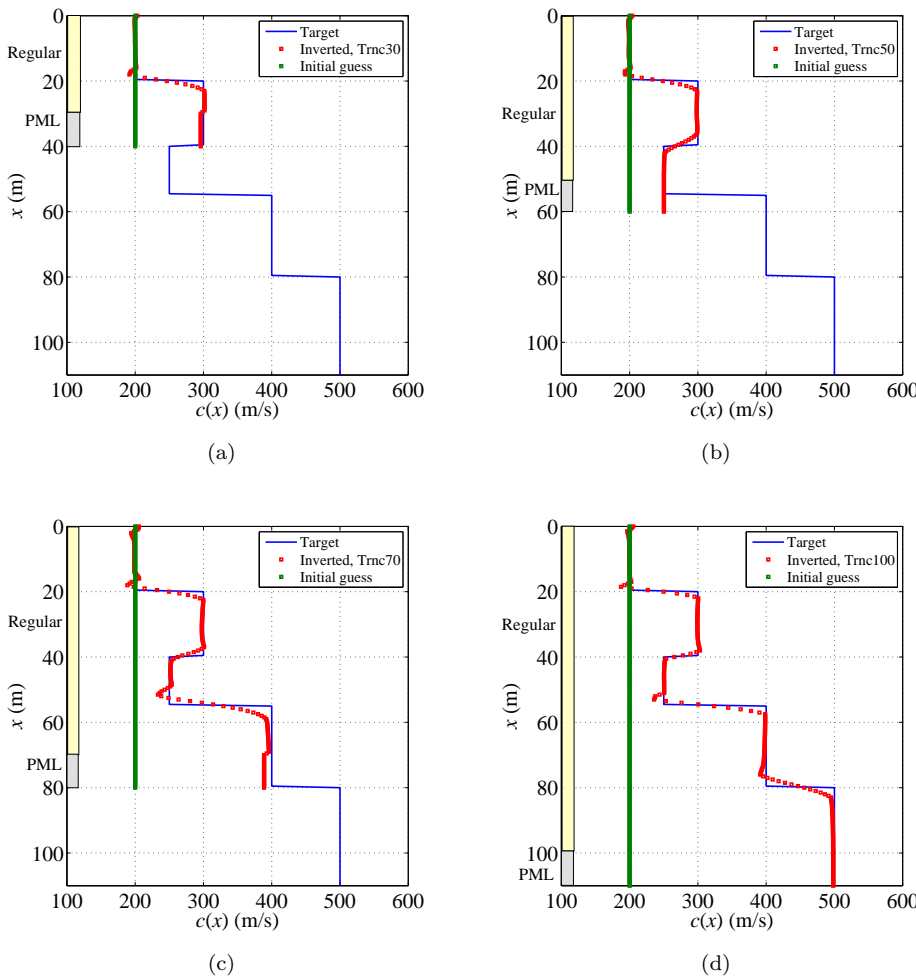


Figure 12. Target, initial guess, and estimated wave velocity profiles $c(x)$ with PML location at (a) 30m; (b) 50m; (c) 70m; (d) 100m; observation period T is optimized; measured data are noise-free.

6. Conclusions

We discussed a PDE-constrained optimization approach for reconstructing the material profile of a one-dimensional heterogeneous semi-infinite medium, truncated by a Perfectly-Matched-Layer (PML), based on surface measurements of its response to surface excitation. The PML was introduced to accommodate the truncation of the semi-infinite extent and absorb the outgoing waves traveling beyond the truncation interface. The underlying numerical scheme was based on a new displacement-stress mixed finite element formulation in the time domain developed recently [16]. As discussed therein, the mixed PML formulation results in nearly perfect wave absorbing performance, avoiding convoluted time integration schemes, which arise when conventional displacement-based finite elements are used.

The PML-endowed PDEs are used within a PDE-constrained optimization framework to resolve the inverse medium problem. In order to alleviate the inherent ill-posedness of the inverse problem, we explored both Tikhonov (TN) and Total Variation (TV) regularization. Both schemes recovered smooth target profiles excellently. For sharply-varying profiles, the TN scheme exhibited limitations, whereas the TV scheme showed good performance. To improve on the ability to recover sharp profiles, we suggested a regularization factor continuation scheme, which tunes the regularization factor at each inversion iteration. The continuation scheme

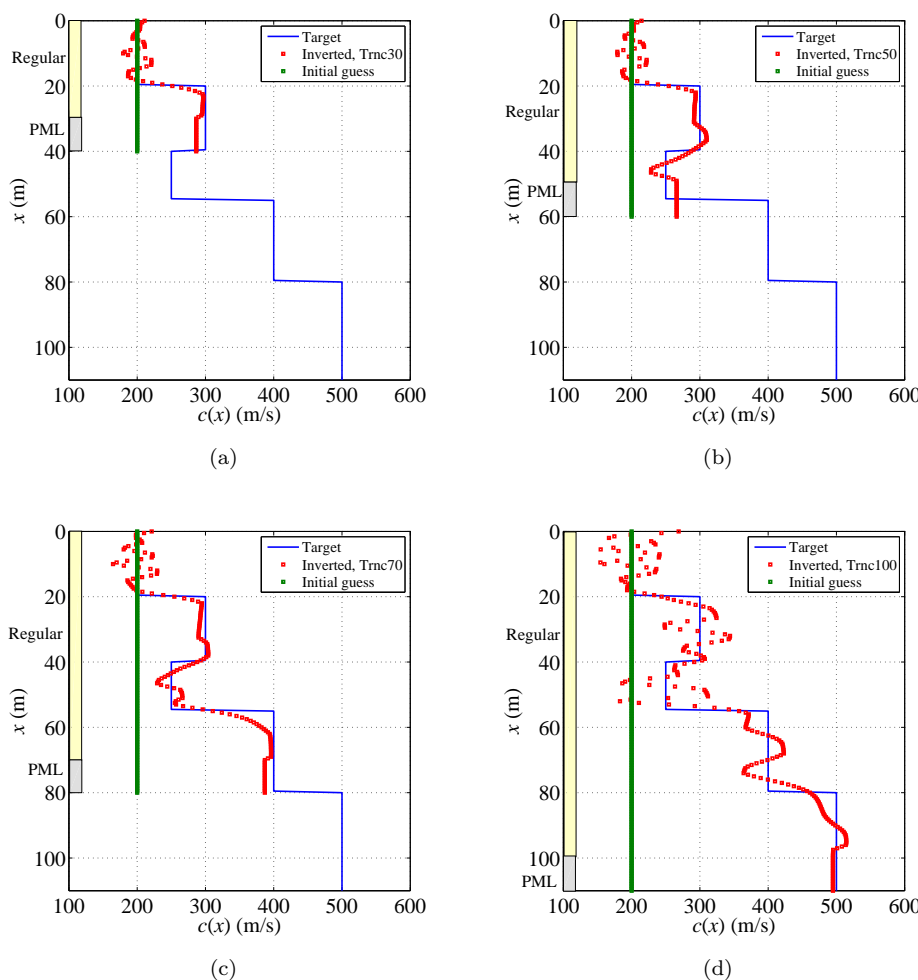


Figure 13. Target, initial guess, and estimated wave velocity profiles $c(x)$ with PML location at (a) 30m; (b) 50m; (c) 70m; (d) 100m; observation period T is optimized; measured data with 20% Gaussian noise.

works quite effectively in recovering sharp profiles even when the regularization factor is initially large. We used both noise-free and noisy data to demonstrate the algorithmic performance. Finally, we showed that, as long as the observation period remains limited, per (79), the PML can be placed anywhere, without concern about the presence of homogeneity past the truncation interface. This is a significant advantage over local absorbing boundaries, which, by construction, result in reflections from the truncation interface, and call for additional and costly treatment in order to ensure the validity of the recovered profiles. Extensions to higher dimensions follow the very lines described herein and will be reported in the future.

7. Acknowledgment

Partial support for the authors research has been provided by the National Science Foundation under grant awards CMS-0348484. This support is gratefully acknowledged.

References

- [1] Chan T F and Tai X C. 2003 Identification of discontinuous coefficients in elliptic problems using total variation regularization. *SIAM J Sci Comput*; **25**(3): 881–904
- [2] Akcelik V. 2002 Multiscale Newton-Krylov methods for inverse acoustic wave propagation. *Doctoral dissertation*, Carnegie Mellon University, Pittsburgh, PA, USA.
- [3] Akcelik V, Biros G and Ghattas O. 2002 Parallel multiscale Gauss-Newton-Krylov methods for inverse wave propagation. *Proceedings of the 2002 ACM/IEEE conference on Supercomputing*. p 1–15.
- [4] Akcelik V, Biros G, Ghattas O, Long K and Waanders B. 2003 A variational finite element method for source inversion for convective-diffusive transport. *Finite Elements in Analysis and Design*; **39**(8): 683–705.
- [5] Biros G and Ghattas O. 1999 Parallel Newton-Krylov Methods for PDE-constrained optimization. *Proceedings of Supercomputing*, Portland, Oregon.
- [6] Engquist B and Majda A. 1977 Absorbing boundary conditions for the numerical simulation of waves. *Mathematics of computation*; **31**(139): 629–651.
- [7] Higdon R. 1991 Absorbing boundary conditions for elastic waves. *Geophysics*; **56**(2): 231–241.
- [8] Kallivokas L and Lee S. 2004 Local absorbing boundaries of elliptical shape for scalar waves. *Computer methods in applied mechanics and engineering*; **193**: 4979–5015.
- [9] Givoli D and Keller J. 1989 A finite element method for large domains. *Computer methods in applied mechanics and engineering*; **76**: 41–66.
- [10] Givoli D and Keller J. 1990 Non-reflecting boundary conditions for elastic waves. *Wave motion*; **12**(3): 261–279.
- [11] Givoli D and Vigdergauz S. 1993 Artificial boundary conditions for 2D problems in geophysics. *Computer methods in applied mechanics and engineering*; **110**(1–2): 87–101.
- [12] Chew W and Liu Q. 1996 Perfectly matched layers for elastodynamics: A new absorbing boundary condition. *Journal of computational acoustics*; **4**(4): 341–359.
- [13] Collino F and Tsogka C. 2001 Application of the perfectly matched absorbing layer model to the linear elastodynamic problem in anisotropic heterogeneous media. *Geophysics*; **66**(1): 294–307.
- [14] Hastings F, Schneider J and Broschat S. 1996 Application of the perfectly matched layer (PML) absorbing boundary condition to elastic wave propagation. *The Journal of the Acoustical Society of America*; **100**(5): 3061–3069.
- [15] Basu U and Chopra A. 2004 Perfectly matched layers for transient elastodynamics of unbounded domains. *International journal for numerical methods in engineering*; **59**: 1039–1074.
- [16] Kang J and Kallivokas L. 2008 Total wavefield-based inversion in PML-truncated domains. *6th International Conference on Inverse Problems in Engineering: Theory and Practice*. Journal of Physics: Conference Series **135**: 012055.
- [17] Lions J. 1971 *Optimal Control of Systems Governed by Partial Differential Equations*. Springer Verlag, Berlin, Heidelberg, New York.
- [18] Gunzburger M and Manservigi S. 1999 The velocity tracking problem for Navier-Stokes flows with bounded distributed controls. *SIAM Journal on Control and Optimization*; **37**(6): 1913–1945.
- [19] Gunzburger M and Manservigi S. 2000 Analysis and approximations of the velocity tracking problem for Navier-Stokes flows with distributed control. *SIAM Journal on Numerical Analysis*; **37**(5): 1481–1512.
- [20] Tikhonov A. 1963 Solution of incorrectly formulated problems and the regularization method. *Soviet Math. Doklady*; **4**: 1035–1038.
- [21] Rudin L, Osher S, Fatemi E. 1992 Nonlinear total variation based noise removal algorithms. *Physica D*; **60**: 259–268.
- [22] Vogel C. 2002 *Computational Methods for Inverse Problems*. SIAM, Frontiers in Applied Mathematics.
- [23] Carey G and Oden J. 1983 *Finite elements - A second course*. Vol. II., Prentice Hall, Englewood Cliffs, NJ.
- [24] Brezzi F and Fortin M. 1991 *Mixed and Hybrid Finite Element Methods*. Springer Verlag, Berlin.
- [25] Bathe k. 1996 *Finite element procedures*. Prentice-Hall, Englewood Cliffs, NJ.
- [26] Rao S. 1996 *Engineering Optimization*. John Wiley & Sons, Inc.
- [27] Nocedal J. and Wright S. 1999 *Numerical Optimization*. Springer Verlag, New York.
- [28] Hansen P and O’Leary D. 1993 The use of the L-curve in the regularization of discrete ill-posed problems. *SIAM Journal on Scientific Computing*; **14**(6): 1487–1503.
- [29] McCarthy P. 2003 Direct analytic model of the L-curve for Tikhonov regularization parameter selection. *Inverse Problems*; **19**: 643–663.
- [30] Na S-W and Kallivokas L F. 2009 Direct time-domain soil profile reconstruction for one-dimensional semi-infinite domains. *Soil Dynamics and Earthquake Engineering*; **29**(6): 1016–1026